HHS Public Access

Author manuscript

J Immunol. Author manuscript; available in PMC 2019 July 01.

Published in final edited form as:

J Immunol. 2018 July 01; 201(1): 19–30. doi:10.4049/jimmunol.1800295.

CD4 T cell affinity diversity is equally maintained during acute and chronic infection Chronic infection fails to alter T cell affinity diversity

Rakieb Andargachew[*], **Ryan J. Martinez**[†], **Elizabeth M. Kolawole**[‡], and **Brian D. Evavold**[§,1]

[*]Department of Microbiology and Immunology, Emory University, Atlanta, GA, 30322.

[†]School of Medicine, Emory University, Atlanta, GA, 30322.

[‡] [§]Division of Microbiology and Immunology, Department of Pathology, University of Utah, Salt Lake City, UT, 84112.

Abstract

T cell receptor (TCR) affinity for peptide major histocompatibility complex (pMHC) dictates the functional efficiency of T cells and their propensity to differentiate into effectors and form memory. However, in the context of chronic infections it is unclear what the overall profile of TCR affinity for antigen is and if it differs from acute infections. Using the comprehensive affinity analysis provided by the 2-dimensional (2D) micropipette adhesion frequency assay (2D-MP) and the common indirect affinity evaluation methods of MHC class II tetramer and functional avidity, we tracked IA^b $GP_{61–80}$ specific cells in the mouse model of acute (Armstrong) and chronic (clone 13) LCMV infection. In each response, we show CD4 T cell population affinity peaks at the effector phase and declines with memory. Of interest, the range and average relative 2D affinity was equivalent between acute and chronic infection, indicating chronic antigen exposure did not skew TCR affinity. In contrast, functional and tetramer avidity measurements revealed divergent results and lacked a consistent correlation with TCR affinity. Our findings highlight the immune system maintains a diverse range in TCR affinity even under the pressures of chronic antigen stimulation.

Introduction

One key parameter regulating T cell activation and functional differentiation in the CD4 T cell response is TCR affinity for antigen. Affinity between receptor and ligand has often been determined using surface plasmon resonance (SPR) measurements (1, 2). However, the need for soluble forms of TCR and pMHC has made the use of this assay impractical for tracking the affinity of large numbers of antigen specific polyclonal T cells in an ongoing immune response. As a result insights into TCR:pMHC affinity and how it instructs the T cell response during an infection have relied on the use of monoclonal TCRs and altered peptide ligands (APLs) with SPR defined affinities (3–5). Polyclonal TCR affinity analysis on the other hand has depended on ex vivo functional avidity and pMHC tetramer staining

[1]Correspondence to: Dr. Brian D. Evavold, University of Utah, Division of Microbiology and Immunology, Department of Pathology, Salt Lake City, UT, 84112. brian.evavold@path.utah.edu, Phone: 801-585-9689.

assays for indirect estimation of TCR affinity based on the positive correlation between these methods and SPR affinity measurements in monoclonal TCR systems (6–10). Hence in functional avidity assays, T cells able to mount functional responses by cytokine production, proliferation or cytotoxic activities in response to low dose antigen have generally possessed TCRs with high affinity for antigen (1, 3, 11). Similarly, the increased staining or avidity of T cell clones for tetramerized pMHC has been correlated to the inherently high affinity interaction between monomeric TCR and pMHC (12).

During an immune response, acute antigen exposure models that have examined both monoclonal and polyclonal populations have demonstrated T cell clones with increased avidity for tetramer and a high functional avidity are preferentially expanded in primary and secondary responses and are selected to become memory cells (6, 7, 9, 13–15). The observed narrowing of the affinity diversity of antigen specific cells to preferentially enrich for high affinity T cell clones has been equated to a form of T cell affinity/avidity maturation (16). In contrast, experiments in chronic infections demonstrated the loss of high avidity clones and later enrichment of lower avidity cells suggesting a decrease in TCR affinity under continuous antigen experience and selection for a T cell affinity profile distinct from the one generated during an acute response (17, 18). As these observations stem from unrelated models that have yet to probe the same antigen specificity and affinity evolution under acute and chronic antigen exposure, it is unclear if affinity skewing actually differs under these conditions. Furthermore, tetramer and functional avidity assays have shown bias towards sampling the highest affinity fraction of the antigen specific repertoire potentially missing the full breadth and diversity in a full polyclonal response to infection (19, 20).

Re-evaluation of polyclonal T cell affinity profiles using the more comprehensive analysis of affinity provided by the 2D-MP assay has now shifted our understanding of TCR affinity breadth and the prevalence and contribution of high and low affinity T cells during a polyclonal immune response (19, 21–23). This microscopy based assay measures monomeric TCR:pMHC affinity at the single cell level with the TCR anchored in its natural T cell membrane context and pMHC coated on a surrogate antigen presenting cell hence providing a 2-dimentional affinity analysis highly predictive of T cell function (24–27). Mounting data highlight low affinity and tetramer negative CD4 clones participate in the immune response, form functional memory and can comprise a larger portion of the antigen specific compartment for a given epitope (3, 19, 23, 28, 29). Affinities ranging from 100–1000 fold have been shown for various antigens in differing immune responses, indicating the immune system maintains a wide breadth of affinities with all possessing the capacity to undergo clonal expansion and form memory (19, 21–23, 27). Although skewing towards high or low affinities has been noted in some models (19, 23), 2D affinity characterization of a polyclonal CD4 T cell response to chronic infection is lacking. In comparison to an acute infection, understanding how the chronic infection environment shifts and shapes the host's antigen specific CD4 T cell populations' TCR affinity diversity can prove beneficial in CD4 T cell therapies aimed at rescuing immune responses in chronic infections (30, 31).

To understand the evolution of T cell affinity and functional responses during infection, we directly compared polyclonal CD4 TCR affinity to the same MHC II (IA^b) restricted $GP_{61–80}$ epitope in the well-studied LCMV model of acute Armstrong (ARM) and chronic

clone 13 (CL13) infections. Although they lead to different infection outcomes, the two viruses share CD4 and CD8 T cell epitopes allowing for a direct comparison of T cell responses across the two models (32). As the majority of the CD4 T cells target the $GP_{61–80}$ peptide with a lower frequency of cells being specific to other minor epitopes, we focused our studies on this immunodominant response (33). 2D-MP, TCR tetramer avidity, tetramer half-life and functional avidity measurements were used to compare the biophysical TCR:pMHC binding and functional characteristics of CD4 T cells as they transitioned from peak effectors to memory cells. Our overall findings demonstrate CD4 TCR affinity diversity is equally maintained under acute and chronic infection with early effectors and late memory CD4 T cells in acute infection having 2D affinities identical to their chronic infection counterparts. Despite the dominance of high affinity cells at the peak of the response, in both acute and chronic infection overall affinity decreased at memory paralleling antigen clearance. Functional and pMHCII tetramer avidity and half-life measurements lacked a consistent correlation to 2D affinity measurements confirming TCR affinity contributes to but is not the sole parameter read out by tetramer and functional avidity assays. As affinity skewing of the CD4 T cell response is similar between acute and chronic infection, our data indicate other regulators modulate T cell function in chronic infection to limit immune pathology without altering affinity diversity in the CD4 T cell response. Hence therapeutic interventions may be able to recover CD4 T cell responses without the need to increase the breadth of TCR affinity.

Materials and Methods

Mice and virus infection

C57BL/6 (B6) mice were purchased from the National Cancer Institute (NCI) and Charles River. B-cell deficient (Ighm−/−) (34) mice on the B6 background were purchased form Jackson Laboratories. For acute and chronic LCMV infection, 6–10 week old female mice were intraperetonially injected with 2×10^5pfu Armstrong or intravenously infected with 2×10^6 pfu CL13 respectively (32, 35–37). Virus stocks were kindly provided by Dr. Rafi Ahmed's lab at Emory University, Atlanta, GA. All animals were housed at the Emory University Department of Animal Resources facility and all experiments were performed in accordance with the guidelines for the Care and Use of Laboratory animals under Emory University Institutional Animal Care and Use Committee approved protocols.

Intracellular cytokine staining: Functional avidity

Splenocytes isolated from infected mice were plated at 2×10^6 cells per tested $GP_{61–80}$ peptide concentration (GLKGPDIYKGVYQFKSVEFD – synthesized on a Prelude Peptide Synthesizer (Protein Technologies)). Tested concentrations ranged from 100μM to 1nM at ten-fold dilutions. Cells were incubated for six hours at 37° C in T cell culture media and 5% CO2 in the presence of 10μg/ml berfeldin A (MP Biomedicals). T cell media contained RPMI 1640 (Mediatech), 10% heat inactivated FBS (Hyclone), 10 mM HEPES buffer (Mediatech), 2mM L-glutamine (Mediatech), 50μM 2-mercaptoethanol (2ME) (Sigma), and 100μg/ml gentamicin (Mediatech). Samples incubated without peptides were used as baseline control while PMA (20nM; Fisher Biotech) and ionomycin (1μM; Sigma) activation served as a positive control. Cells were washed and stained with surface antibodies for 30

minutes on ice in FACS staining buffer containing phosphate buffered saline (PBS) (Mediatech), 0.1% bovine serum albumin (BSA) (Fisher Scientific), and 0.05% sodium azide (Sigma). Staining antibodies included anti-CD4 FITC (RM4–5; Tonbo biosciences/eBioscience), anti-CD11b PerCP Cy5.5 (M1/70; BD), anti-CD11c PerCP Cy5.5 (HL3; BD), anti-CD19 PerCP Cy5.5 (ID3; BD), anti-CD3ε PECF594 (145–2C11; BD), anti-CD44 AF700 (IM7; LifeTechnologies), anti-CD27 V450 (LG3.A10; BD), Viability Ghost Dye Violet (Tonbo/eBiosciences), anti-PD-1 BV605 (29F.1A12; Biolegend), and anti-CD8 BV785 (53–6.7; Biolegend). Using Invitrogen FIX and PERM or BD Cytofix/Cytoperm kits, cells were fixed and permeabilized in accordance with manufacturer's protocols. Intracellular antibody staining was performed for 30 min on ice using the manufacturers' permeabilization solution and anti-IFNγ APC Cy7 (XMG1.2; BD), anti-TNFα PE Cy7 (MP6-XT22; Biolegend), anti-IL-2 APC (JES6–5H4; BD) antibodies. Aliquots of unstained splenocytes were used to obtain total cell and different population counts using AccuCheck microbeads (Invitrogen). Cells were washed and kept on ice until flow cytometry was carried out using a FACSVerse or LSR II (Beckton Dickson). Data analysis was performed using FlowJo software (Tree Star). To generate avidity curves and derive EC_{50}, the frequency of cytokine positive cells (with frequency of unstimulated control subtracted) at the 100μM concentration was used as the maximal cytokine producer frequency and equated to a 100% with the remaining frequencies at lower peptide doses normalized to this maximal response as previously described (14, 38). Normalized values were graphed against log transformed peptide concentrations and the data fitted to a nonlinear regression (log (agonist) vs normalized response) using GraphPad Prism 7 analysis software.

TCR staining

TCR expression differences were quantified using the anti-TCRβ clone H57–597 PE antibody (eBioscience). Briefly, a few million splenocytes from infected mice were surface stained on ice for 30 minutes with anti-CD11b PerCP Cy5.5 (M1/70; BD), anti-CD11c PerCP Cy5.5 (HL3; BD), anti-CD19 PerCP Cy5.5 (ID3; BD), 7AAD (BD), anti-CD3ε PE CF594 (145–2C11; BD), anti-CD44 PE Cy7 (IM7; Biolegend), anti-CD62L APC Cy7 (MEL-14; BD), anti-CD27 V450 (LG3.A10; BD), anti-CD4 BV510 (RM4–5; Biolegend), anti-PD-1 BV605 (29F.1A12; Biolegend), and anti-CD8 BV785 (53–6.7; Biolegend) antibodies along with the anti-TCRβ antibody. Cells were washed and kept on ice until flow cytometry was carried out using a LSR II (Beckton Dickson). Using the FlowJo software (Tree Star), TCR, CD4 and forward scatter (FSC-A) mean fluorescence intensities (MFIs) of $CD4+CD44^{hi}$ (antigen experienced) and $CD4+CD44^{lo}CD62+$ (naïve) cells was quantified and compared between the two infections per experiment. QuantiBRITE PE quantification beads (BD Biosciences) were used per manufacturer instructions to determine the number of TCRs per cell. For further comparison between infections and across different time points, MFI of antigen experienced cells was normalized to the naïve population within the same sample and quantified as % of naïve ((antigen experienced MFI/naïve MFI) x 100) (39).

Tetramer avidity

Tetramer staining was performed with splenocytes at a density of 2×10^6 cells (100μl volume) per tested concentration (10μg/ml – 0.01μg/ml at 10 fold dilutions, 5–0.05μg/ml at 10 fold dilutions, 2.5μg/ml, 0.25μg/ml) of the PE conjugated IA^b $GP_{66–77}$ tetramer acquired

from the NIH Tetramer Core Facility at Emory University, Atlanta, GA. Labeling was done in T cell media at room temperature for 1 hour. As control, IA^b $hCLIP_{103–117}$ tetramer (NIH Tetramer Core) was used to stain the samples at 10μg/ml. Cells were washed with cold staining buffer and surface stained on ice for 30 minutes prior to sample acquisition on a FACSVerse or LSRII flow cytometer. Aliquots of unstained splenocytes were used to obtain total cell and different population counts using AccuCheck microbeads (Invitrogen). Antibodies used for surface staining included anti-CD11b PerCP Cy5.5 (M1/70; BD), anti-CD11c PerCP Cy5.5 (HL3; BD), anti-CD19 PerCP Cy5.5 (ID3; BD), 7AAD (BD), anti-CD3ε PE CF594 (145–2C11; BD), anti-CD44 PE Cy7 (IM7; Biolegend), anti-CD62L APC Cy7 (MEL-14; BD), anti-CD27 V450 (LG3.A10; BD), anti-CD4 BV510 (RM4–5; Biolegend), anti-PD-1 BV605 (29F.1A12; Biolegend), and anti-CD8 BV785 (53–6.7; Biolegend). Data analysis was performed using FlowJo software (Tree Star). To generate dose response curves and derive EC_{50}, the frequency of tetramer stained cells at 10μg/ml concentration was used as the maximal response and equated to a 100% with the remaining frequencies at lower tetramer doses normalized to this maximal frequency as previously described (14, 18, 38). Normalized values were graphed against log transformed tetramer concentrations and the data fitted to a nonlinear regression (log (agonist) vs normalized response) using GraphPad Prism 7 analysis software.

Tetramer decay

Splenocytes were stained with tetramer at 10μg/ml for 1hr at room temperature at a cell density of 20×10^6 cells in 1ml of FACS staining buffer (0.05% sodium azide). Cells were washed with ice cold buffer to remove excess tetramer and kept on ice until an aliquot (2×10^6 splenocytes in FACS buffer) was incubated with 100μg/ml of the anti-IA/IE (M5/114.15.2: eBioscience) blocking antibody at room temperature. Decay was measured at 3hrs, 2hrs, 1.5hrs, 1hr, 40mins, 20mins, and 10mins post antibody addition. The tetramer stained sample without blocking antibody addition was used for the 0min time point. Incubation was done in a staggered manner starting with the 3hrs and decreasing to the last time point with all incubations ending concurrently and all samples completed at the same time (begin the 3hrs incubation, 1hr later start the 2hr incubation and so on). Cells were then washed with ice cold staining buffer to remove excess blocking antibody and kept cold during all washes. Staining for surface markers was performed on ice with anti-CD11b PerCP Cy5.5 (M1/70; BD), anti-CD11c PerCP Cy5.5 (HL3; BD), anti-CD19 PerCP Cy5.5 (ID3; BD), 7AAD (BD), anti-CD3ε PE CF594 (145–2C11; BD), anti-CD44 PE Cy7 (IM7; Biolegend), anti-CD62L APC Cy7 (MEL-14; BD), anti-CD27 V450 (LG3.A10; BD), anti-CD4 BV510 (RM4–5; Biolegend), anti-PD-1 BV605 (29F.1A12; Biolegend), and anti-CD8 BV785 (53–6.7; Biolegend) antibodies. Cells were kept on ice until sample acquisition was done on a LSRII flow cytometer. Mean fluorescence intensity of tetramer positive cells (control IA^b $hCLIP_{103–117}$ staining used to draw positive gate) was normalized to tetramer staining intensity at time zero ((MFI at time (y)/MFI at zero) x 100) and the normalized MFI was graphed against time. The data was fitted to a one-phase exponential decay curve using Prism 7 analysis software (Graphpad) and the half-life was determined accordingly (40, 41).

2D micropipette adhesion frequency assay (2D-MP)

The relative 2D affinity of polyclonal IA^b $GP_{66–77}$ specific cells was measured using the previously characterized 2-dimensional micropipette adhesion frequency assay (19, 26). In this 2D assessment, the frequency of adhesion between ligand (pMHC on human red blood cell (hRBC)) and receptor (TCR on T cell) carrying cells held on opposing micropipettes was observed using an inverted Zeiss microscope. The presence of adhesion was denoted by the interaction induced stretching of the highly flexible RBC membrane as the two cells were separated after an equilibrium contact time of two seconds. To serve as a surrogate APC, the RBC was first biotinylated (Biotin-x-NHS; Calbiochem) then incubated with streptavidin (ThermoFisher) followed by the addition of biotinylated pMHC monomers (IA^b $GP_{66–77}$ or a control monomer (IA^b $hCLIP_{103–117}$, MTB IA^b $Ag85B_{280–294}$ and IA^b $ESAT\text{-}6_{1–19}$ and Influenza IA^b $NP_{311–325}$). T cell samples were prepared from splenocytes by $CD4+CD44^{hi}$ cell enrichment through CD4 T cell purification using EasySep mouse CD4 T cell negative selection kit (STEM CELL Technologies) and the simultaneous depletion of CD62L+ cells through the addition of biotinylated anti-CD62L antibody (MEL-14: eBioscience at 10ug/ml per 1×10^8 cells) to the manufacturer recommended volume of the isolation cocktail. For 2D affinity measurements of tetramer positive cells, CD4+CD62- enriched samples were stained with tetramer (described in tetramer avidity methods) and sorted on a FACSAriaII (BD Biosciences). To determine relative 2D affinity, 30 independent 2 second contacts were tested per T cell to generate an adhesion frequency value (Pa(2s)). Cells showing an adhesion frequency above 10% at the highest pMHC coating densities (>1000/μm^2) were considered antigen reactive (previously identified cutoff (19, 21)). Cells exhibiting 100% adhesion were further resolved using lower pMHC densities until frequency values below 90% were obtained (27). The adhesion frequency was used to derive the relative 2D affinity of the cell with the following equation. AcKa = -ln (1-Pa(2s)) / $m_r m_l$ where m_r and m_l represent receptor (TCR) and ligand (pMHC) density per area (μm^2), Pa(2s) is the adhesion frequency at the 2s equilibrium contact time, Ac is the contact area (kept constant) and AcKa is the 2D affinity (in μm^4) (24). TCR and pMHC density per cell was determined using QuantiBRITE PE quantification beads (BD Biosciences) per manufacturer instructions and staining of TCR with anti-mouse TCRβ PE antibody (H57–597; BD Biosciences) and MHC staining with anti-IA/IE antibody (M5/114/15/2; eBioscience) both at saturating concentrations. Calculations of molecules per area were done by dividing the number of TCR and pMHC per cell by the respective surface areas (hRBC 140 μm^2, T cell -during assay measured diameter of an individual T cell and the surface area equation of a sphere) (26). A total of 70–400 cells were tested per sample with 20–70 binders/antigen specific cells used to derive the geometric mean affinity for a given population.

Statistical analysis

Statistical significance of measured values was determined with Ordinary-One Way ANOVA, Turkey's multiple comparison, Sidak's multiple comparison, and two-tailed parametric Student's t-tests with ROUT outlier test (Q=1%) used to eliminate outliers all using the Prism 7 Software (GraphPad). Statistical significance indicated as ns = no significance, * P > 0.05, ** P > 0.01, *** P > 0.001, and **** P > 0.0001.

Results

Chronic antigen stimulation leads to T cell dysfunction but maintains tetramer positive cells at a number comparable to the acute response

In the LCMV B6 model, the Armstrong virus causes an acute infection that lasts 8–10 days whereas CL13 persists 40–80 days in serum and spleen but remains in tissues like the brain and kidney (42–44). Chronic antigen exposure leads to CD4 T cell dysfunction early in CL13 infection and results in a faulty memory pool that is unable to mount a secondary response (36, 45). To compare and contrast how the duration of antigen exposure alters the frequency and number of IA^b restricted $GP_{61–80}$ specific CD4 T cells, we assessed the T_H1 cytokine response and the overall prevalence of pMHCII tetramer positive cells (i.e higher affinity cells) at time points that corresponded to prior and post viral antigen clearance. CL13 infection led to the increased and sustained expression of the inhibitory and recent antigen experience marker PD-1 on $GP_{61–80}$ specific IFNγ producing T_H1 (Fig. 1A) and pMHCII tetramer positive cells early in the infection (Fig. 1B). PD-1 expression was upregulated at the early effector (day 8 post infection (d8)) and chronic stage (d35) of the CL13 response confirming continuous antigen exposure as compared to the acute infection. A marked decrease in PD-1 expression was noted at d120 indicating viral clearance from serum and spleen at this late time point (Fig. 1A, 1B). As is the hallmark of the chronic infection, the dysfunction in the T_H1 response was observed with a significant reduction in the frequency and number of IFNγ positive (Fig. 1C) and polyfunctional IFNγ, TNFα, and IL-2 co-producing CD4 T cells (Supplemental Fig. 1A–C) as compared to the more robust acute response (32, 36). However, the two responses had an equal prevalence of epitope specific tetramer positive CD4 T cells at the later time points (d35 and d120) and only differed in the number of expanded effectors at d8 (Fig. 1D) (36, 45). Although this suggested the inhibitory environment in CL13 infection limited early CD4 T cell expansion, the decay in this population occurred relatively slower with a similar number of tetramer positive T cells maintained between d8 and d35 and a significant contraction occurring at d120 with antigen clearance (Fig. 1D). In contrast, a continuous decline in tetramer positive cells was observed as the acute response progressed from the expansion of peak d8 effectors to the formation and maintenance of early (d35) and late (d120) memory cells. Hence, more contraction and culling of antigen-specific cells occurred throughout memory long after clearance of viral antigen. The decay pattern in the T_H1 population (Fig. 1C) mirrored the observed decrease in tetramer positive cell numbers (Fig. 1D) in both acute and chronic infection and confirmed previous observations of time dependent memory CD4 T cell decline in acute infections (14, 38, 46). As pMHCII tetramers are partial to high affinity cell detection, these data suggested high affinity CD4 T cells are retained in the presence of antigen with chronic infection (18) and that their decline in the absence of antigen was not unique to chronic antigen stimulation but occurred in response to acute infection as well.

CD4 T cell affinity peaks at effector phase and declines equally with memory in acute and chronic infection

As low affinity cells are expected to participate in the immune response and potentially dominate (18, 23) our observation of a decline in the high affinity (tetramer positive) antigen specific CD4 T cell population in both acute and chronic infection alluded to a possible

decrease in the overall affinity of the response in the progression towards viral clearance. To evaluate if affinity declines in the total antigen specific population, inclusive of tetramer positive and negative CD4 T cells, we used the 2D-MP to measure single cell CD4 TCR affinity. In the 2D-MP assay, the adhesion between TCR and pMHC on micropipette anchored CD4 T cells and pMHC coated human red blood cells (hRBCs) was visually assessed using an inverted microscope (19, 24, 26, 27). Adhesion or binding was evidenced as the elongation of the flexible RBC membrane as the two cells were brought in contact and separated sequentially (Supplemental Fig. 2A). These adhesion or binding events along with surface density of TCR and pMHC were used to generate a relative 2D affinity for individual T cells and the geometric mean affinity was used to compare different populations. To perform these measurements, we enriched for CD4+CD62L- T cells to maximize the frequency of antigen experienced CD4+CD44^{hi} cells within the sample (Supplemental Fig. 2B). Determining the adhesion frequency to the IA^{b} GP$_{66–77}$ monomer as compared to a control non-LCMV monomer tested the LCMV specificity of individual T cells within each sample (Supplemental Fig. 2C). Using this method, high and low affinity cells were detected in both the acute and chronic infection at all the time points tested with a >1000 fold affinities represented in each response. However, the peak TCR affinity of the polyclonal response occurred at d8 with both infections showing increased prevalence of higher affinity CD4 T cells before a decline occurred in the transition to memory time points (Fig. 2A,B). Of interest, at both the d8 peak effector and d120 memory time points the acute (ARM Fig. 2A) and chronic (CL13 Fig. 2B) infections generated an antigen specific population with equivalent average affinities (ARM;CL13 d8 – 1×10^{-4} μm^4; 2×10^{-4} μm^4 and d120 – 8×10^{-6} μm^4; 3×10^{-6} μm^4). While the Armstrong population affinity steadily declined to the d120 time point, the CL13 responders maintained the same high affinity effector levels between d8 and d35 and only declined in the transition between d35 and d120 (Fig. 2C). Therefore, in the acute and chronic infections, the CD4 T cell population affinity was highest during the effector response with antigen presence maintaining a larger frequency of higher affinity T cells as observed with tetramer staining frequency and numbers. Viral clearance in both infections resulted in a lower affinity memory CD4 T cell population concurrent with a decline in tetramer positive T cells.

Identification of virus-specific CD4 T cells by 2D-MP revealed a greater frequency of responding T cells than determined using pMHCII tetramer, as previously noted (19, 23). Employing an in vivo limiting dilution assay along with the Nur77GFP reporter mice with peptide antigen delivered in CFA, we had reported the number and affinity of naïve antigen specific precursors inclusive of lower affinity T cells for several antigens (23). Lower affinity, tetramer negative precursors were found to dominate the naïve population for all the tested epitopes including the LCMV epitope studied in this work. In the naïve repertoire tetramer negative IA^{b} GP$_{66–77}$ specific lower affinity T cells outnumbered tetramer positive high affinity precursors by >3 fold and similarly dominated during Armstrong and CL13 infections reaching a seven-fold difference at d120 (Fig. 2D,E). To validate that tetramer preferentially stains higher affinity CD4 T cells, we sorted pMHCII tetramer positive cells from d7 Armstrong infected mice to greater than 99% enrichment (Supplemental Fig. 2D) using fluorescence activated cell sorting (FACS) and measured their 2D affinity. Compared to the total antigen-specific CD4 T cell population, the sorted tetramer positive T cells had a

ten-fold higher affinity and demonstrated a narrowed affinity range (Fig. 2F). Based on this and previous observations from LCMV and myelin oligodendrocyte glycoprotein (MOG) specific tetramer positive cells (19), 1×10^{-4} μm^4 was used as the threshold 2D affinity cutoff for tetramer binding, with higher and lower affinity TCRs falling above and below this line, respectively. As the population affinity decreased below this threshold during memory (Fig. 2A–C), the increasing disparity between the antigen specific cell frequencies detected by 2D-MP and tetramer largely occurred from pMHCII tetramer missing lower-affinity TCRs.

In a Friend virus protracted infection model, antigen presentation by activated B-cells was necessary for the expansion and over-representation of lower affinity T cell clonotypes and the decay in high affinity T cells late in the infection (18). To determine if the affinity decline in the LCMV model can also be attributed to a B-cell role and thus abolished in an environment devoid of B-cells, we measured 2D affinity of IA^b $GP_{66–77}$ specific CD4 T cells in Armstrong infected B-cell deficient mice (Ighm −/−). Similar to the infection of wild type (WT) B6 mice, Ighm−/− mice demonstrated a decrease in average TCR affinity between effector (d8) and memory (d85) T cells (Fig. 2G – trending significance $p = 0.0522$). 2D-MP identified more antigen specific cells than pMHCII tetramer during both the effector and memory stages of the response with the transition from the d8 five-fold frequency difference to the twenty-four-fold change by d85 confirming the increased prevalence of low affinity cells at the later time point (Figure 2h). The increased frequency of low affinity cells at memory coupled with the drop in 2D affinity demonstrated the skewing to lower affinity cells can occur in the absence of B-cells. While this does not rule out a possible role for B-cells in the B6 model it suggested other mechanisms also contribute to the observed decay in affinity.

Tetramer avidity changes in chronic infection in the absence of TCR affinity differences

Overall, the skewing to lower affinity T cells in the acute response was in opposition to other findings of affinity maturation or selective enrichment of higher affinity cells at memory (6–9). As these observations were made using pMHC tetramers as surrogate readouts for TCR affinity, we assessed tetramer avidity in the two infections for a comparison to these previous studies and our 2D affinity data. As measures of TCR affinity, 2D-MP and pMHCII tetramer avidity analysis require an accounting of TCR density and total number of receptors per cell (12, 26, 47). Accordingly, we monitored TCR expression levels in acute and chronic infection with the TCR specific anti-TCRβ (clone H57–597) monoclonal antibody. As performed with our 2D-MP protocols we used quantification beads to determine the number of TCRs on $CD44^{hi}$ cells. CD4 T cells in chronic infection had a higher TCR expression at d35 whereas d8 and d120 numbers remained equivalent to Armstrong responders (Fig. 3A). A lack of TCR downregulation between d8 and d35 in CL13 infection contributed to this observed difference. Of note, TCR numbers decreased past antigen clearance time points within each infection indicating TCR downregulation can occur independent of antigen presence. This finding was analogous to a study that revealed TCR downregulation as a programmed event set early during antigen encounter but manifesting later in the response despite the absence of antigen (39). Although the contribution of the CD4 co-receptor was found to be minimal in binding to pMHCII (12, 20, 48, 49), we next assessed CD4 expression levels on $CD44^{hi}$ cells relative to the naïve population (Fig. 3B.) The difference

was limited to d8 effectors with identical expression patterns observed between acute and chronic infections at d35 and d120 (Fig. 3C). Flow cytometry analysis of forward scatter (FSC-A) was also used to assess T cell size and identify TCR and CD4 density differences. In both infections, activated T cells were larger at the peak of the response and reduced in size towards memory (Fig. 3D). CL13 specific cells at d8 were larger than their Armstrong counterparts while d35 and d120 cells were of equivalent size. Although in CL13 infection exhausted CD8 T cells were previously found to be smaller in size compared to late memory cells (50), CD4 T cell size at d120 was not significantly different between exhausted and memory cells despite showing a similar trend. The cell size data together with the TCR expression changes suggested potential TCR density differences between early and late time points in both the acute and chronic infection. While normalized in our 2D-MP measurements, these differences can affect tetramer avidity (12, 39).

To measure pMHCII tetramer avidity, we stained splenocytes with decreasing concentrations of IA^b $GP_{66–77}$ tetramer and used IA^b $CLIP_{103–117}$ control tetramer to determine the frequency of cells with specific staining. The frequency at the highest tetramer concentration was defined as the maximal frequency (100%), the data normalized accordingly and fitted to a dose-response curve (Fig. 4A,C) for quantification of tetramer EC_{50} concentrations (Fig. 4B,D). Tetramer avidity remained unchanged between effector and memory cells in the Armstrong response (Fig. 4A,B) where in contrast, avidity changes were noted in the chronic infection with d35 CD4 T cells showing increased tetramer avidity (Fig. 4C,D). A comparison of acute and chronic responders showed CD4 T cells in the CL13 response had significantly higher tetramer avidity at all the time points tested (Fig. 4E). Given that the TCR expression difference across the two infections was only limited to d35, the d8 and d120 increased avidity in CL13 suggested a CD4 and TCR number independent effect thus we next assessed 2D affinity. For a fair comparison between 2D affinity and tetramer avidity, we excluded tetramer negative T cells from our 2D-MP analysis using the tetramer binding threshold affinity (1×10^{-4} μm^4) to group single cell measurements into high affinity tetramer binders and tetramer negative cells. In both acute and chronic infection, the average 2D affinity of antigen specific cells falling above this threshold remained unchanged throughout each infection and across the two responses (Fig. 4F–G). In the Armstrong infection, this relative 2D affinity mimicked the observed static tetramer avidity, while in the CL13 response, tetramer avidity changes occurred despite the equivalent 2D affinities measured at each time point. The lack of TCR number and 2D affinity differences at d8 and d120 suggested the two responses generate a CD4 T cell population with comparable affinities while other affinity and TCR number independent factors influenced tetramer avidity (EC_{50}). CD4 co-receptor's role in binding pMHCII has previously been shown to be negligible (12, 20, 48, 49) and does not explain differences in avidity and affinity measurements identified here.

Tetramer half-life similar between memory and exhausted CD4 T cells

A direct correlation between TCR affinity and TCR:pMHC interaction half-life have previously been observed, where high affinity T cells had a longer interaction duration with pMHC displaying antigen presenting cells (4, 51). To determine if pMHCII tetramer interaction half-life correlated to avidity or 2D affinity measurements, we next performed

tetramer decay assays. After pMHCII staining of samples from acutely or chronically infected mice, tetramer labeled cells were incubated with an anti-MHC II antibody that binds dissociated tetramer and prevents rebinding to TCR (6, 39, 52). The decay in tetramer staining intensity was measured over time, and normalized to the signal detected at time 0. The data was fitted to a one-phase exponential decay non-linear regression and half-life determined accordingly (Fig. 5A,B) (40, 41). To avoid the inadvertent early skewing to a negative signal (MFI) that occurs with grouping tetramer positive and negative polyclonal populations together, decay in tetramer staining intensity was measured for T cells falling in the tetramer positive gate established using the control tetramer. To validate our analysis we compared the frequency of tetramer positive cells detected at every decay time point. The frequency of tetramer positive cells detected at time 0 was similar to the frequency at all other time points during the assay, indicating the decay in tetramer MFI does not lead to a loss in detection of antigen-specific T cells (Supplemental Fig. 3A–C, data not shown). Using this analysis method, tetramer decay measurements in both the Armstrong and CL13 response showed a similar interaction half-life across all infection time points (Fig. 5A,B, Supplemental Fig. 3D–E). Equivalent pMHCII tetramer half-lives were also noted between acute and chronic infection at all points of comparison (Figure 5c) aligning half-life measurements with 2D affinity but not pMHCII tetramer avidity.

Exhausted CD4 T cells have a lower functional avidity compared to memory cells

Functional avidity is often used to infer the affinity of a polyclonal T cell response with a high functional avidity generally predicting the presence of TCRs with a greater affinity for pMHC (3). Furthermore, this ex-vivo testing of a virus-specific CD4 T cell populations' ability to respond to decreasing doses of cognate antigen allows for a comparison of their sensitivity and potential to generate a functional response in-vivo (53). In this dose-response assay, the frequency of cytokine producing CD4 T cells at each dose of cognate antigen was normalized to the frequency observed at the highest peptide concentration (100uM), and the data fitted to a nonlinear curve for deriving half-maximal effective concentration (EC_{50}) values. With acute infection (Fig. 6A), IFNγ producing $GP_{61–80}$ specific CD4 T cells showed increased functional avidity in the transition from effectors to early memory but no further increase at late memory, contrary to previous findings (14). A similar functional avidity increase was also detected in CD4 T cells responding to CL13 infection (Fig. 6B). Despite this similar trend, the CD4 T cells in the acute infection had a significantly higher functional avidity compared to the chronic responders as seen with EC_{50} measurements of IFNγ (Fig. 6C). Within each infection, the antigen sensitivity seen with IFNγ producers was recapitulated with IL-2 (Fig. 6D) and TNFα (data not shown) producers. However between acute and chronic responders, unlike the IFNγ avidity difference seen at all time points, IL-2 (Fig. 6D) and TNFα (data not shown) avidity equalized at the d120 time point. Collectively, the data demonstrated virus-specific CD4 T cells increase sensitivity to antigen in response to acute and chronic infection but initial activation conditions set degree of sensitivity. Furthermore, this increased sensitivity can occur without an accompanying increase in 2D affinity or pMHCII tetramer avidity.

Discussion

In an infection setting, a T cell's potential for activation, expansion, cytokine production and survival as a memory cell is dependent on TCR affinity as well as other inflammatory environment incited selective pressures (14, 52, 54, 55). In this study, using the 2D-MP assay, we sought to further our understanding of how the antigen specific CD4 T cell population's average TCR affinity changes under the pressures of acute and chronic infection in the well-studied LCMV model. In LCMV and other infections, CD4 T cells adept at controlling acute infections demonstrate robust cytokine production and form long-lived memory that protects the host against subsequent infections. However, in chronic infections as seen with the LCMV mouse model as well as the human pathogens HIV and HCV, continuous exposure to high antigen levels render CD4 T cells functionally exhausted and with altered T helper and memory differentiation outcomes (32, 35, 45, 56–59). While the efficacy of the CD4 response in acute infections has previously been correlated to the enrichment of high affinity/avidity T cells (6, 9, 14, 38), recent observations in retroviral infection models have demonstrated the chronic response to be enriched in lower affinity/avidity clones late in the infection (17, 18).

Our data highlight under acute and chronic infection CD4 T cell affinity diversity is equally maintained. Both responses expanded peak effector CD4 T cells of equivalent 2D affinities and the average affinity of the antigen specific population similarly declined with antigen clearance. Although both high and low affinity T cells expanded to infection and later contracted, the relative abundance of each population changed depending on the stage of the immune response. At the peak of the effector response and in the presence of antigen high affinity cells were more prevalent (18) in both acute and chronic infection. However with antigen clearance increased contraction of high affinity T cells (tetramer positive) (60) and a potential outgrowth of lower affinity (18, 61) clones gave way to a lower affinity T cell dominated memory population in both Armstrong and CL13 infection. As previously noted (19, 23), the 2D-MP detected more antigen specific cells (2–7 fold higher) in both acute and chronic infection compared to pMHCII tetramer which selectively identified higher affinity cells. In evidence of this affinity bias, we found pMHCII tetramer positive cells had a ten-fold higher average 2D affinity and spanned a narrower affinity range compared to the tetramer positive and negative inclusive sample. As the CD4 T cell population affinity declined with memory, more antigen specific cells were identified using 2D-MP than pMHCII tetramer. At the naïve precursor level, a similar skewing to lower affinity cells was previously observed for $GP_{61–80}$ specific CD4 T cells which showed a 3:1 bias (23) before settling in to the observed 7:1 ratio at memory. This would suggest the immune system maintains and resets the ratio of low to higher affinity T cells back to this similar pre-infection hierarchy that existed prior to infection.

Active mechanisms that promote affinity diversity and maintain lower affinity cells in the immune system have previously been proposed (8, 18, 62). In the CD4 T cell response to Friend virus protracted infection model, a similar decrease in affinity and enrichment for lower affinity cells was observed late in the infection (18). While showing this similar skewing to lower affinity cells occurred in the chronic LCMV CL13 model, we also observed this phenomenon was not unique to chronic infection as the acute response shared

this progression from a peak affinity at effector time points before a decrease in overall affinity at memory. Of interest, the decline in overall T cell affinity was dependent on B-cell antigen presentation in the Friend virus infection model. In our 2D affinity measurements of Armstrong infected B-cell deficient Ighm−/− mice a similar affinity decline between effector and memory cells suggested other T cell intrinsic and extrinsic factors regulated CD4 T cell population affinity. Of note, in a previous characterization of Armstrong infection in Ighm−/− mice, CD4 T cell memory numbers and cytokine production was found significantly reduced when compared to the WT response (63). While the poor secondary lymphoid architecture in Ighm−/− mice also contributed towards the deficit in CD4 memory, transient depletion of B-cells in WT mice identified a clear B-cell role in sustaining CD4 T cell memory numbers during the T cell contraction phase (64). These findings together with our observed affinity decline both in the presence and absence of B-cells suggest these cells maintain memory CD4 T cell numbers as a whole and likely without partiality towards higher or lower affinity clones in the LCMV model. Redirection of CD4 T helper differentiation and prevention of immune pathology in Friend virus infection was also dependent on B-cells unlike the LCMV chronic response (58, 59) hence confirming the potential role of other mechanisms in the enrichment of lower affinity cells in the LCMV model. However, further investigation is needed to identify said mechanisms and the contribution of B-cells towards this event without the confounding factors present in Ighm−/− mice. Of interest, the lack of affinity differences between acute and chronic LCMV infection suggested the shift towards a T_{FH} response in CL13 also occurred independent of a differential TCR affinity skewing. In agreement with our observations, the potential for differentiation into T_{FH} cells has been noted for high to low TCR affinity interactions with antigen dose playing a significant role in driving monoclonal T cells down a T_{FH} or alternative differentiation path (55, 58, 65).

The CD27/CD70 co-stimulatory pathway has previously been reported as a mechanism that insures memory T cell survival and TCR affinity diversity through maintenance of lower affinity T cells in the antigen specific repertoire (8, 62, 66). Characterization of co-stimulatory molecules on pMHCII tetramer positive memory and exhausted T cells in the same LCMV models of acute and chronic infection has shown increased CD27 expression on exhausted CD4 T cells (36). Although we also noted CL13 specific early effectors had increased CD27 expression compared to Armstrong responders, tetramer positive and total $CD44^{hi}$ cells did not sustain high CD27 expression levels in the progression to lower affinity memory time points (data not shown). Despite the early difference in CD27 expression, acute and chronic responders demonstrated identical 2D affinities in the high affinity T cell population (tetramer positive) at all time points tested. The total population also equally shifted to a lower affinity population at late memory making CD27 expression an unlikely mechanism leading to low affinity T cell enrichment. However, direct approaches that abrogate CD27/CD70 interaction may further clarify if this pathway plays a role in the observed decline in CD4 T cell affinity.

Contrary to our 2D affinity observations, selection into the memory pool has previously been correlated with increased population affinity as measured by avidity for pMHCII tetramer, longer tetramer binding half-lives and a higher functional avidity (6, 9, 14, 38). Given the correlation between these measurements and monomeric TCR:pMHC affinity, memory is

thought to enriches for higher affinity/avidity T cells resulting in T cell affinity maturation (7, 13, 16, 67). Our tetramer avidity measurements in acute and chronic infection revealed neither population enriched for higher avidity cells in the progression to memory time points. In fact, pMHCII tetramer avidity remained identical in the transition from peak effectors to memory cells in the Armstrong infection while a higher avidity was measured at d35 in the CL13 response. However TCR expression difference can be a confounding factor when comparing avidity within each infection. Between Armstrong and CL13 responders, the similar TCR expression in d8 and d120 samples allowed for a direct comparison of avidity with the data demonstrating increased avidity in the CL13 response. Our reanalysis of average 2D affinities for T cell populations falling above the 1×10^{-4} 2D affinity cutoff for tetramer binding showed affinity to be static in each high affinity (tetramer positive) response and equivalent between acute and chronic infection. This suggested TCR affinity independent mechanisms might be playing a role in the observed tetramer avidity differences. CD4 has no contribution toward binding pMHCII tetramer (12, 48, 49) and expression differences were limited to d8 samples thus co-receptor did not explain the increased avidity. Tetramer staining relies on the binding of multiple TCRs to the same pMHCII tetramer complex with one interaction increasing the likelihood of a second TCR:pMHC binding hence the avidity (10, 40). T cell activation induced changes in TCR clustering, membrane lipid raft organization and decreased membrane stiffness or enhanced fluidity can lead to altered tetramer binding capabilities at the T cell surface and could be factors different in the inflammatory environment with continuous antigen stimulation (68–70). Memory T cell population skewing based on increased pMHCII tetramer interaction half-life and in the absence of a tetramer avidity based enrichment has previously been noted (52). In our comparisons, tetramer half-life measurements remained equivalent over the course of each response and between acute and chronic responders showing a correlation to 2D affinity measurements of the high affinity CD4 T cell population.

As antigen specific peak T_H1 effectors progressed down the differentiation path to early and late memory cells, a stepwise increase in functional avidity was noted in Armstrong infection (14, 38). Although functional avidity remained similar between early and late memory cells, our data also demonstrated a shift towards increased antigen sensitivity in the transition from peak effectors to early memory cells. The increased antigen sensitivity occurred in the absence of comparable 2D affinity, tetramer avidity and half-life changes. Other studies of monoclonal and polyclonal responses have also reported a similar disassociation between TCR affinity and functional avidity (14, 37, 67). Under continuous antigen exposure, exhausted T_H1 cells also increased functional avidity as the immune response progressed towards antigen clearance but the degree of sensitivity was significantly reduced as compared to the robust IFNγ response in Armstrong infection. Antigen dose, the inflammatory environment and the upregulation of inhibitory receptors in the CL13 response can dampen T cell activation and functional responses (53, 54).

Overall, our 2D affinity findings highlight CD4 TCR affinity diversity in the antigen specific polyclonal population is equally maintained under the pressures of acute and chronic infection with both systems expanding CD4 T cell populations of identical 2D affinities. High affinity T cells dominated peak effector populations, whereas increased prevalence of lower affinity cells coincided with antigen clearance. A correlation between functional and

tetramer avidity measurements and 2D micropipette based affinity analysis was not consistent confirming the influence of TCR affinity independent mechanisms on these assays. Identification of parameters that predict and correlate with the efficacy of a CD4 T cell's response are critical in tailoring therapies and vaccines towards effectively combating acute and chronic infections. While our 2D TCR affinity, pMHCII tetramer avidity and half-life analysis did not differentiate CD4 memory cells from their exhausted counterparts, our data confirmed increased functional avidity better correlated to the T cell response difference between acute and chronic infection and the generation of functional memory. We now show in chronic infection, the immune response can maintain a population with an intact TCR affinity distribution that can be targeted by therapies that restore antigen sensitivity and boost CD4 T cell functionality. Future studies are required to identify immune mechanisms that are in place for maintaining this affinity diversity and to further elucidate the role of high and low affinity cells within the immune response. Comparisons of as yet unmeasured TCR:pMHC kinetic and biophysical parameters can explain the response difference in the two infections and provide better correlates to protection and futures targets for immunotherapies.

Supplementary Material

Refer to Web version on PubMed Central for supplementary material.

Acknowledgement

We would like to thank Matthew A. Williams and J. Scott Hale for their helpful comments on this manuscript. We thank all members of the Evavold lab for useful scientific discussions and L.A. Lawrence for maintaining mouse colonies. We thank the Ahmed lab for providing virus stocks and the National Institute of Health Tetramer Core Facility for providing pMHC reagents. We also would like to acknowledge the Emory Children's Pediatric Research Center flow cytometry core facility for performing cell sorting.

Source of Support

This work was supported by National Institute of Health Grants R01 NS071518, R01 AI096879, and National Institute of Health Training Grant T32 AI007610 (B.D.E).

Abbreviations

pMHC (pMHCII)	peptide major histocompatibility complex (II)
2D	two-dimensional
2D-MP	two-dimensional micropipette adhesion frequency assay
LCMV	Lymphocytic choriomeningitis virus
ARM	Armstrong virus
CL13	clone 13 virus
dpi (d.p.i)	days post infection
Tet +, Tet -	tetramer positive, tetramer negative

References

1. Matsui K, Boniface JJ, Steffner P, Reay PA, and Davis MM. 1994 Kinetics of T-cell receptor binding to peptide/I-Ek complexes: correlation of the dissociation rate with T-cell responsiveness. Proc. Natl. Acad. Sci. U. S. A 91: 12862–12866. [PubMed: 7809136]
2. Corr M, Slanetz AE, Boyd LF, Jelonek MT, Khilko S, al-Ramadi BK, Kim YS, Maher SE, Bothwell AL, and Margulies DH. 1994 T cell receptor-MHC class I peptide interactions: affinity, kinetics, and specificity. Science 265: 946–949. [PubMed: 8052850]
3. Zehn D, Lee SY, and Bevan MJ. 2009 Complete but curtailed T-cell response to very low-affinity antigen. Nature 458: 211–214. [PubMed: 19182777]
4. Daniels MA, Teixeiro E, Gill J, Hausmann B, Roubaty D, Holmberg K, Werlen G, Holländer GA, Gascoigne NR, and Palmer E. 2006 Thymic selection threshold defined by compartmentalization of Ras/MAPK signalling. Nature 444: 724–729. [PubMed: 17086201]
5. Stone JD, Chervin AS, and Kranz DM. 2009 T-cell receptor binding affinities and kinetics: impact on T-cell activity and specificity. Immunology 126: 165–176. [PubMed: 19125887]
6. Savage PA, Boniface JJ, and Davis MM. 1999 A kinetic basis for T cell receptor repertoire selection during an immune response. Immunity 10: 485–492. [PubMed: 10229191]
7. Busch DH, and Pamer EG. 1999 T cell affinity maturation by selective expansion during infection. J. Exp. Med 189: 701–710. [PubMed: 9989985]
8. Baumgartner CK, Yagita H, and Malherbe LP. 2012 A TCR affinity threshold regulates memory CD4 T cell differentiation following vaccination. J. Immunol 189: 2309–2317. [PubMed: 22844120]
9. Malherbe L, Hausl C, Teyton L, and McHeyzer-Williams MG. 2004 Clonal selection of helper T cells is determined by an affinity threshold with no further skewing of TCR binding properties. Immunity 21: 669–679. [PubMed: 15539153]
10. Altman JD, Moss PAH, Goulder PJR, Barouch DH, McHeyzer-Williams MG, Bell JI, McMichael AJ, and Davis MM. 1996 Phenotypic Analysis of Antigen-Specific T Lymphocytes. Science 274: 94–96. [PubMed: 8810254]
11. Gottschalk RA, Hathorn MM, Beuneu H, Corse E, Dustin ML, Altan-Bonnet G, and Allison JP. 2012 Distinct influences of peptide-MHC quality and quantity on in vivo T-cell responses. Proc. Natl. Acad. Sci. U. S. A 109: 881–886. [PubMed: 22223661]
12. Crawford F, Kozono H, White J, Marrack P, and Kappler J. 1998 Detection of antigen-specific T cells with multivalent soluble class II MHC covalent peptide complexes. Immunity 8: 675–682. [PubMed: 9655481]
13. Whitmire JK, Benning N, and Whitton JL. 2006 Precursor frequency, nonlinear proliferation, and functional maturation of virus-specific CD4+ T cells. J. Immunol 176: 3028–3036. [PubMed: 16493061]
14. Williams MA, Ravkov EV, and Bevan MJ. 2008 Rapid culling of the CD4+ T cell repertoire in the transition from effector to memory. Immunity 28: 533–545. [PubMed: 18356084]
15. Cukalac T, Chadderton J, Handel A, Doherty PC, Turner SJ, Thomas PG, and La Gruta NL. 2014 Reproducible selection of high avidity CD8+ T-cell clones following secondary acute virus infection. Proc. Natl. Acad. Sci. U. S. A 111: 1485–1490. [PubMed: 24474775]
16. Kedl RM, Kappler JW, and Marrack P. 2003 Epitope dominance, competition and T cell affinity maturation. Curr. Opin. Immunol 15: 120–127. [PubMed: 12495743]
17. Lichterfeld M, Yu XG, Mui SK, Williams KL, Trocha A, Brockman MA, Allgaier RL, Waring MT, Koibuchi T, Johnston MN, Cohen D, Allen TM, Rosenberg ES, Walker BD, and Altfeld M. 2007 Selective depletion of high-avidity human immunodeficiency virus type 1 (HIV-1)-specific CD8+ T cells after early HIV-1 infection. J. Virol 81: 4199–4214. [PubMed: 17287271]
18. Merkenschlager J, Ploquin MJJ, Eksmond U, Andargachew R, Thorborn G, Filby A, Pepper M, Evavold B, and Kassiotis G. 2016 Stepwise B-cell-dependent expansion of T helper clonotypes diversifies the T-cell response. Nature Communications 7 (10281): 1–13.
19. Sabatino JJ, Huang J, Zhu C, and Evavold BD. 2011 High prevalence of low affinity peptide-MHC II tetramer-negative effectors during polyclonal CD4+ T cell responses. J. Exp. Med 208: 81–90. [PubMed: 21220453]

20. Nepom GT 2012 MHC class II tetramers. J. Immunol 188: 2477–2482. [PubMed: 22389204]
21. Hood JD, Zarnitsyna VI, Zhu C, and Evavold BD. 2015 Regulatory and T effector cells have overlapping low to high ranges in TCR affinities for self during demyelinating disease. J. Immunol 195: 4162–4170. [PubMed: 26385521]
22. Kersh AE, Edwards LJ, and Evavold BD. 2014 Progression of relapsing-remitting demyelinating disease does not require increased TCR affinity or epitope spread. J. Immunol 193: 4429–4438. [PubMed: 25267971]
23. Martinez RJ, Andargachew R, Martinez HA, and Evavold BD. 2016 Low-affinity CD4+ T cells are major responders in the primary immune response. Nature Communications 7 (13848): 1–10.
24. Chesla SE, Selvaraj P, and Zhu C. 1998 Measuring two-dimensional receptor-ligand binding kinetics by micropipette. Biophys. J 75: 1553–1572. [PubMed: 9726957]
25. Hong J, Persaud SP, Horvath S, Allen PM, Evavold BD, and Zhu C. 2015 Force-Regulated In Situ TCR-Peptide-Bound MHC Class II Kinetics Determine Functions of CD4+ T Cells. J. Immunol 195: 3557–3564. [PubMed: 26336148]
26. Huang J, Zarnitsyna VI, Liu B, Edwards LJ, Jiang N, Evavold BD, and Zhu C. 2010 The kinetics of two-dimensional TCR and pMHC interactions determine T-cell responsiveness. Nature 464: 932–936. [PubMed: 20357766]
27. Zhang S-Q, Parker P, Ma K-Y, He C, Shi Q, Cui Z, Williams CM, Wendel BS, Meriwether AI, Salazar M, and Jiang N. 2016 Direct measurement of T cell receptor affinity and sequence from naïve antiviral T cells. Sci. Transl. Med 8: 341ra377–341ra377.
28. Krummey SM, Martinez RJ, Andargachew R, Liu D, Wagener M, Kohlmeier JE, Evavold BD, Larsen CP, and Ford ML. 2016 Low-affinity memory CD8+ T cells mediate robust heterologous immunity. J. Immunol 196: 2838–2846. [PubMed: 26864034]
29. Martinez RJ, and Evavold BD. 2015 Lower affinity T cells are critical components and active participants of the immune response. Front. Immunol 6: 468–468. [PubMed: 26441973]
30. Aubert RD, Kamphorst AO, Sarkar S, Vezys V, Ha S-JJ, Barber DL, Ye L, Sharpe AH, Freeman GJ, and Ahmed R. 2011 Antigen-specific CD4 T-cell help rescues exhausted CD8 T cells during chronic viral infection. Proc. Natl. Acad. Sci. U. S. A 108: 21182–21187. [PubMed: 22160724]
31. Penaloza-MacMaster P, and Provine NM. 2015 CD4 T Cell depletion substantially augments the rescue potential of PD-L1 blockade for deeply exhausted CD8 T cells. J. Immunol 195: 1054–1063. [PubMed: 26116499]
32. Fuller MJ, Khanolkar A, Tebo AE, and Zajac AJ. 2004 Maintenance, loss, and resurgence of T cell responses during acute, protracted, and chronic viral infections. J. Immunol 172: 4204–4214. [PubMed: 15034033]
33. Dow C, Oseroff C, Peters B, Nance-Sotelo C, Sidney J, Buchmeier M, Sette A, and Mothé BR. 2008 Lymphocytic choriomeningitis virus infection yields overlapping CD4+ and CD8+ T-cell responses. J. Virol 82: 11734–11741. [PubMed: 18829752]
34. Kitamura D, Roes J, Kühn R, and Rajewsky K. 1991 A B cell-deficient mouse by targeted disruption of the membrane exon of the immunoglobulin mu chain gene. Nature 350: 423–426. [PubMed: 1901381]
35. Fuller MJ, and Zajac AJ. 2003 Ablation of CD8 and CD4 T cell responses by high viral loads. J. Immunol 170: 477–486. [PubMed: 12496434]
36. Crawford A, Angelosanto JM, Kao C, Doering TA, Odorizzi PM, Barnett BE, and Wherry EJ. 2014 Molecular and transcriptional basis of CD4(+) T cell dysfunction during chronic infection. Immunity 40: 289–302. [PubMed: 24530057]
37. Shorter SK, Schnell FJ, McMaster SR, Pinelli DF, Andargachew R, and Evavold BD. 2016 Viral escape mutant epitope maintains TCR affinity for antigen yet curtails CD8 T cell responses. PLoS One 11: e0149582–e0149582. [PubMed: 26915099]
38. Kim C, Jay DC, and Williams MA. 2012 Stability and function of secondary Th1 memory cells are dependent on the nature of the secondary stimulus. J. Immunol 189: 2348–2355. [PubMed: 22844122]
39. Gallegos AM, Xiong H, Leiner IM, Sušac B, Glickman MS, Pamer EG, and van Heijst JW. 2016 Control of T cell antigen reactivity via programmed TCR downregulation. Nat. Immunol 17: 379–386. [PubMed: 26901151]

40. Stone JD, Artyomov MN, Chervin AS, Chakraborty AK, Eisen HN, and Kranz DM. 2011 Interaction of streptavidin-based peptide-MHC oligomers (tetramers) with cell-surface TCRs. J. Immunol 187: 6281–6290. [PubMed: 22102724]
41. Laugel B, van den Berg HA, Gostick E, and Cole DKW, Boulter L, Milicic J, Price A, D. Sewell AK 2007 Different T cell receptor affinity thresholds and CD8 coreceptor dependence govern cytotoxic T lymphocyte activation and tetramer binding properties. J. Biol. Chem 282: 23799–23810. [PubMed: 17540778]
42. Wherry EJ, Blattman JN, Murali-Krishna K, van der Most R, and Ahmed R. 2003 Viral persistence alters CD8 T-cell immunodominance and tissue distribution and results in distinct stages of functional impairment. J. Virol 77: 4911–4927. [PubMed: 12663797]
43. Ahmed R, Salmi A, Butler LD, Chiller JM, and Oldstone MB. 1984 Selection of genetic variants of lymphocytic choriomeningitis virus in spleens of persistently infected mice. Role in suppression of cytotoxic T lymphocyte response and viral persistence. J. Exp. Med 160: 521–540. [PubMed: 6332167]
44. Matloubian M, Somasundaram T, Kolhekar SR, Selvakumar R, and Ahmed R. 1990 Genetic basis of viral persistence: single amino acid change in the viral glycoprotein affects ability of lymphocytic choriomeningitis virus to persist in adult mice. J. Exp. Med 172: 1043–1048. [PubMed: 2212940]
45. Brooks DG, Teyton L, Oldstone MB, and McGavern DB. 2005 Intrinsic functional dysregulation of CD4 T cells occurs rapidly following persistent viral infection. J. Virol 79: 10514–10527. [PubMed: 16051844]
46. Homann D, Teyton L, and Oldstone M. 2001 Differential regulation of antiviral T-cell immunity results in stable CD8+ but declining CD4+ T-cell memory. Nat. Med 7: 913–919. [PubMed: 11479623]
47. Wooldridge L, Lissina A, Cole DK, van den Berg HA, Price DA, and Sewell AK. 2009 Tricks with tetramers: how to get the most from multimeric peptide-MHC. Immunology 126: 147–164. [PubMed: 19125886]
48. Xiong Y, Kern P, Chang H, and Reinherz E. 2001 T Cell Receptor Binding to a pMHCII Ligand Is Kinetically Distinct from and Independent of CD4. J. Biol. Chem 276: 5659–5667. [PubMed: 11106664]
49. Hamad AR, O'Herrin SM, Lebowitz MS, Srikrishnan A, Bieler J, Schneck J, and Pardoll D. 1998 Potent T cell activation with dimeric peptide-major histocompatibility complex class II ligand: the role of CD4 coreceptor. J. Exp. Med 188: 1633–1640. [PubMed: 9802975]
50. Wherry JE, Ha S-J, Kaech SM, Haining NW, Sarkar S, Kalia V, Subramaniam S, Blattman JN, Barber DL, and Ahmed R. 2007 Molecular Signature of CD8+ T Cell Exhaustion during Chronic Viral Infection. Immunity 27: 670–684. [PubMed: 17950003]
51. Moreau HD, Lemaître F, Terriac E, Azar G, Piel M, Lennon-Dumenil A-MM, and Bousso P. 2012 Dynamic in situ cytometry uncovers T cell receptor signaling during immunological synapses and kinapses in vivo. Immunity 37: 351–363. [PubMed: 22683126]
52. Kim C, Wilson T, Fischer KF, and Williams MA. 2013 Sustained interactions between T cell receptors and antigens promote the differentiation of $CD4^+$ memory T cells. Immunity 39: 508–520. [PubMed: 24054329]
53. Viganò S, Utzschneider DT, Perreau M, Pantaleo G, Zehn D, and Harari A. 2012 Functional avidity: a measure to predict the efficacy of effector T cells? Clin. Dev. Immunol 2012: 14–14.
54. Kim C, Jay DC, and Williams MA. 2014 Dynamic functional modulation of CD4+ T cell recall responses is dependent on the inflammatory environment of the secondary stimulus. PLoS Pathog. 10: e1004137–e1004137. [PubMed: 24854337]
55. Tubo NJ, and Jenkins MK. 2014 TCR signal quantity and quality in CD4(+) T cell differentiation. Trends Immunol. 35: 591–596. [PubMed: 25457838]
56. Day CL, Kaufmann DE, Kiepiela P, Brown JA, Moodley ES, Reddy S, Mackey EW, Miller JD, Leslie AJ, DePierres C, Mncube Z, Duraiswamy J, Zhu B, Eichbaum Q, Altfeld M, Wherry JE, Coovadia HM, Goulder PJR, Klenerman P, Ahmed R, Freeman GJ, and Walker BD. 2006 PD-1 expression on HIV-specific T cells is associated with T-cell exhaustion and disease progression. Nature 443: 350–354. [PubMed: 16921384]

57. Schulze zur Wiesch J, Ciuffreda D, Lewis-Ximenez L, Kasprowicz V, Nolan BE, Streeck H, Aneja J, Reyor LL, Allen TM, Lohse AW, McGovern B, Chung RT, Kwok WW, Kim AY, and Lauer GM. 2012 Broadly directed virus-specific CD4+ T cell responses are primed during acute hepatitis C infection, but rapidly disappear from human blood with viral persistence. J. Exp. Med 209: 61–75. [PubMed: 22213804]
58. Fahey LM, Wilson EB, Elsaesser H, Fistonich CD, McGavern DB, and Brooks DG. 2011 Viral persistence redirects CD4 T cell differentiation toward T follicular helper cells. J. Exp. Med 208: 987–999. [PubMed: 21536743]
59. Ploquin MJJ, Eksmond U, and Kassiotis G. 2011 B cells and TCR avidity determine distinct functions of CD4+ T cells in retroviral infection. J. Immunol 187: 3321–3330. [PubMed: 21841129]
60. Ertelt JM, Johanns TM, Mysz MA, Nanton MR, Rowe JH, Aguilera MN, and Way SS. 2011 Selective culling of high avidity antigen-specific CD4+ T cells after virulent Salmonella infection. Immunology 134: 487–497. [PubMed: 22044420]
61. Rosenthal KM, Edwards LJ, Sabatino JJ, Hood JD, Wasserman HA, Zhu C, and Evavold BD. 2012 Low 2-dimensional CD4 T cell receptor affinity for myelin sets in motion delayed response kinetics. PLoS One 7: e32562–e32562. [PubMed: 22412888]
62. van Gisbergen KP, Klarenbeek PL, Kragten NA, Unger P-PAP, Nieuwenhuis MBB, Wensveen FM, ten Brinke A, Tak PP, Eldering E, Nolte MA, and van Lier RA. 2011 The costimulatory molecule CD27 maintains clonally diverse CD8(+) T cell responses of low antigen affinity to protect against viral variants. Immunity 35: 97–108. [PubMed: 21763160]
63. Whitmire JK, Asano MS, and Kaech SM. 2009 Requirement of B cells for generating CD4+ T cell memory. J. Immunol 182: 1868–1876. [PubMed: 19201839]
64. Misumi I, and Whitmire JK. 2014 B cell depletion curtails CD4+ T cell memory and reduces protection against disseminating virus infection. J. Immunol 192: 1597–1608. [PubMed: 24453250]
65. Keck S, Schmaler M, Ganter S, Wyss L, Oberle S, Huseby ES, Zehn D, and King CG. 2014 Antigen affinity and antigen dose exert distinct influences on CD4 T-cell differentiation. Proc. Natl. Acad. Sci. U. S. A 111: 14852–14857. [PubMed: 25267612]
66. Hendriks J, Gravestein LA, Tesselaar K, van Lier RA, Schumacher TN, and Borst J. 2000 CD27 is required for generation and long-term maintenance of T cell immunity. Nat. Immunol 1: 433–440. [PubMed: 11062504]
67. Slifka MK, and Whitton JL. 2001 Functional avidity maturation of CD8(+) T cells without selection of higher affinity TCR. Nat. Immunol 2: 711–717. [PubMed: 11477407]
68. Drake DR, and Braciale TJ. 2001 Cutting edge: lipid raft integrity affects the efficiency of MHC class I tetramer binding and cell surface TCR arrangement on CD8+ T cells. J. Immunol 166: 7009–7013. [PubMed: 11390443]
69. Schamel WW, Arechaga I, Risueño RM, van Santen HM, Cabezas P, Risco C, Valpuesta JM, and Alarcón B. 2005 Coexistence of multivalent and monovalent TCRs explains high sensitivity and wide range of response. J. Exp. Med 202: 493–503. [PubMed: 16087711]
70. Thauland TJ, Hu KH, Bruce MA, and Butte MJ. 2017 Cytoskeletal adaptivity regulates T cell receptor signaling. Sci. Signal 10: eaah3737–eaah3737. [PubMed: 28270556]

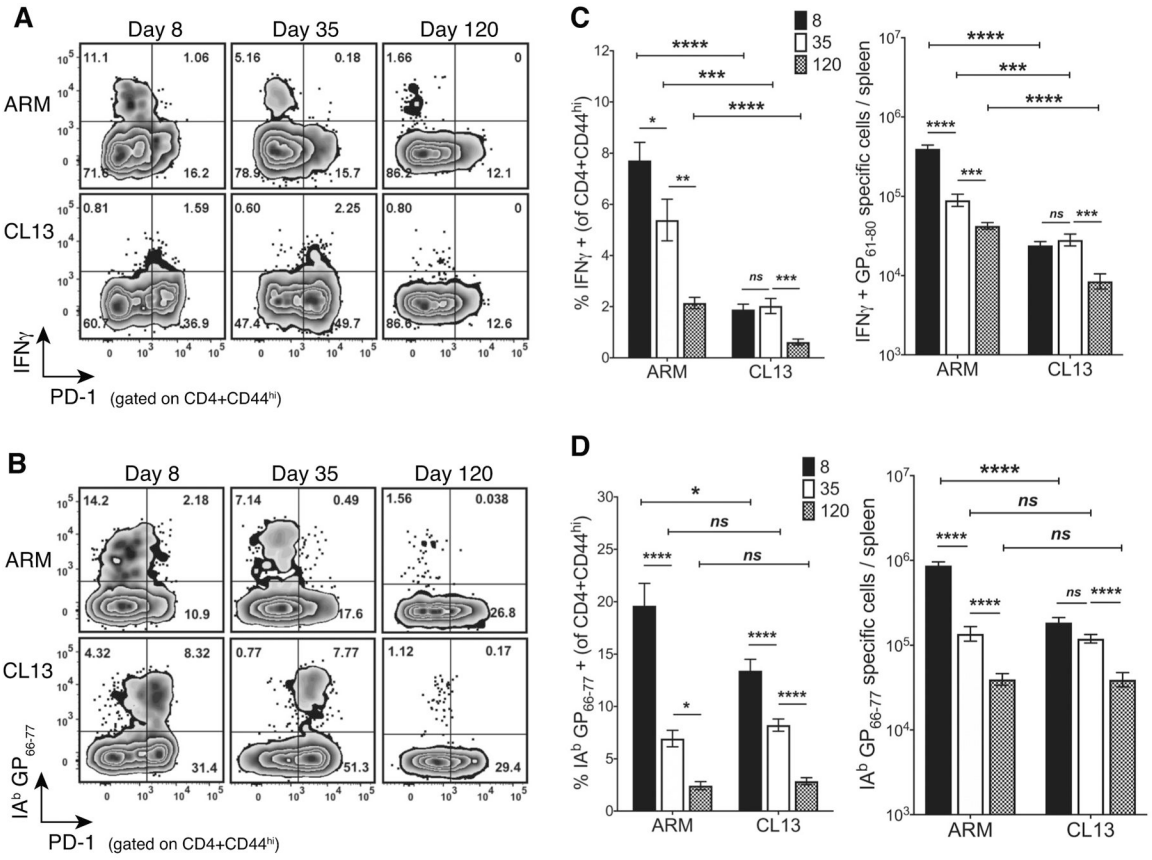

Figure 1. Chronic antigen stimulation leads to T cell dysfunction but maintains tetramer positive cells at a number comparable to the acute response.

(A) A representative flow plot with the frequency of IFNγ and PD-1 expressing cells in ARM and CL13 at the indicated days post infection (dpi) gated on CD4+CD44^{hi} splenocytes. **(B)** A representative flow plot with the frequency of IA^b GP$_{66–77}$ tetramer+ and PD-1 expressing cells under the conditions mentioned in (A). **(C)** Frequency (left) and log transformed absolute numbers (right) of IFNγ producing cells at the time points and infections represented in the flow plot in (A). **(D)** Frequency (left) and log transformed absolute numbers (right) of IA^b GP$_{66–77}$ tetramer+ T cells represented in (B). (C,D) Cumulative data with 3–5 independent experiments and a total n = 7–19 mice/group at n=2–5 mice/experiment/group. Bar graphs with Mean ± SEM. Statistical significance, ns = no significance, * P > 0.05, ** P > 0.01, *** P > 0.001, **** P > 0.0001, Student t-test (ARM vs CL13), Ordinary one-way ANOVA Tukey's multiple comparison test (between dpi - individual infections).

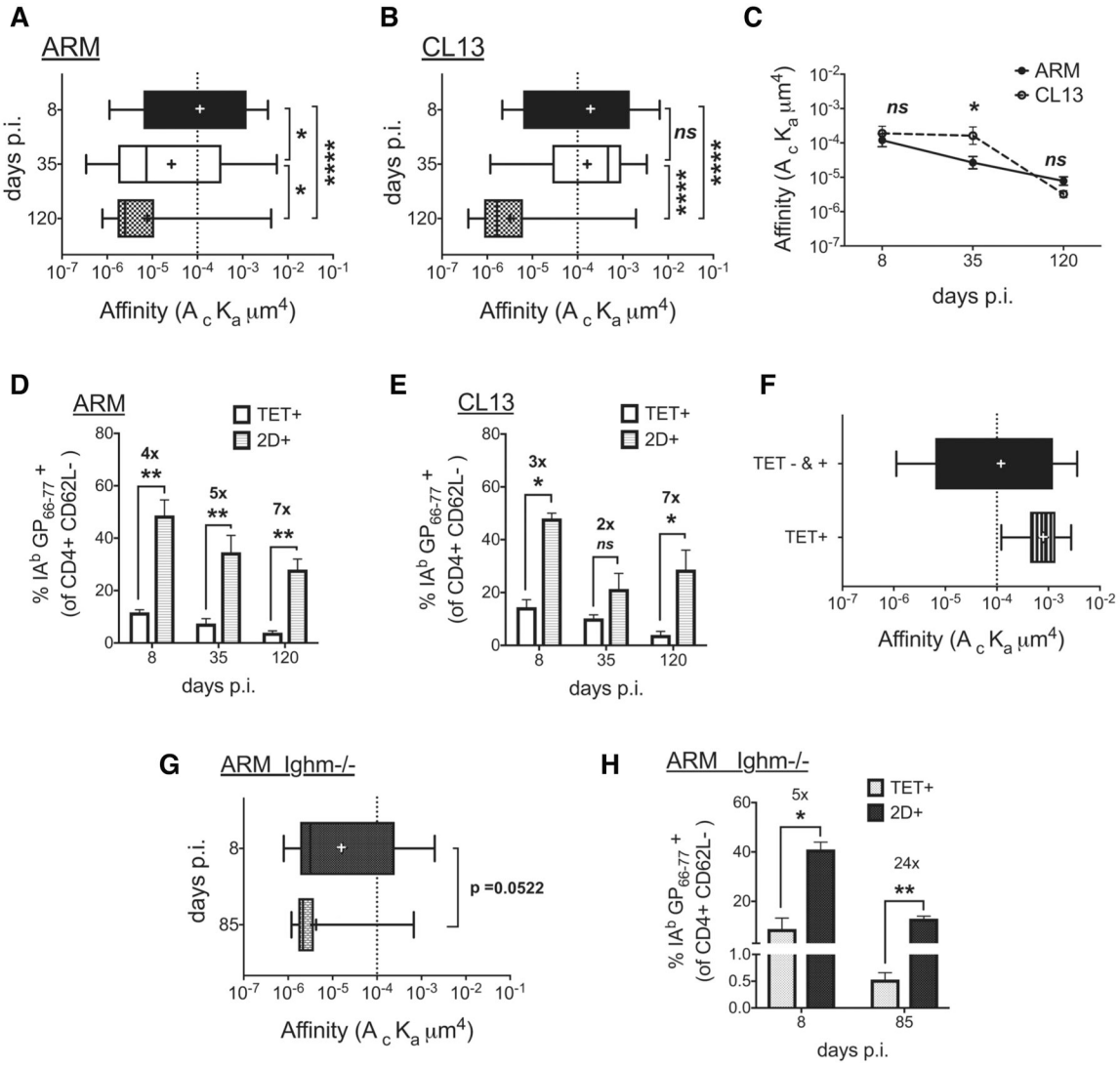

Figure 2. CD4 T cell affinity peaks at effector phase and declines equally with memory in acute and chronic infection.

(A, B) 2D affinity of IA^b $GP_{66–77}$ specific cells in CD4+CD62L- enriched samples from ARM **(A)** and CL13 **(B)** infected splenocytes and a comparison of the two infections **(C)** at the designated days. **(D,E)** A comparison of tetramer and 2D detected frequency of IA^b $GP_{66–77}$ specific cells in above-mentioned samples from **(D)** ARM and **(E)** CL13. **(F)** 2D affinity of sorted tetramer+ and total (tet+ and tet-) CD4+CD62L- cells from d7 ARM infected splenocytes. **(G)** 2D affinity of IA^b $GP_{66–77}$ specific CD4+CD62L- T cells from ARM infected B-cell deficient (Ighm−/−) mice at d8 and d85 dpi with p-value (0.0522). **(H)** Comparison of tetramer and 2D frequency in samples from (G). All data representative of 2–3 independent experiments with splenocytes from 2–3 mice pooled pre-CD4+CD62L- enrichment per time point and per infection. Affinity data log transformed with (+) sign depicting mean affinity in box and whisker graphs with min to max range of measured single cell affinities. Tetramer + high affinity cell cutoff as a dotted line at 1×10^{-4}. Mean + SEM in bar graphs. Statistical significance, ns = no significance, * P > 0.05, ** P > 0.01, *** P >

0.001, **** P > 0.0001, (A,B) Ordinary one-way ANOVA Tukey's multiple comparison test, (C) Sidak's multiple comparison test, (D, E, G, H) Student t-test.

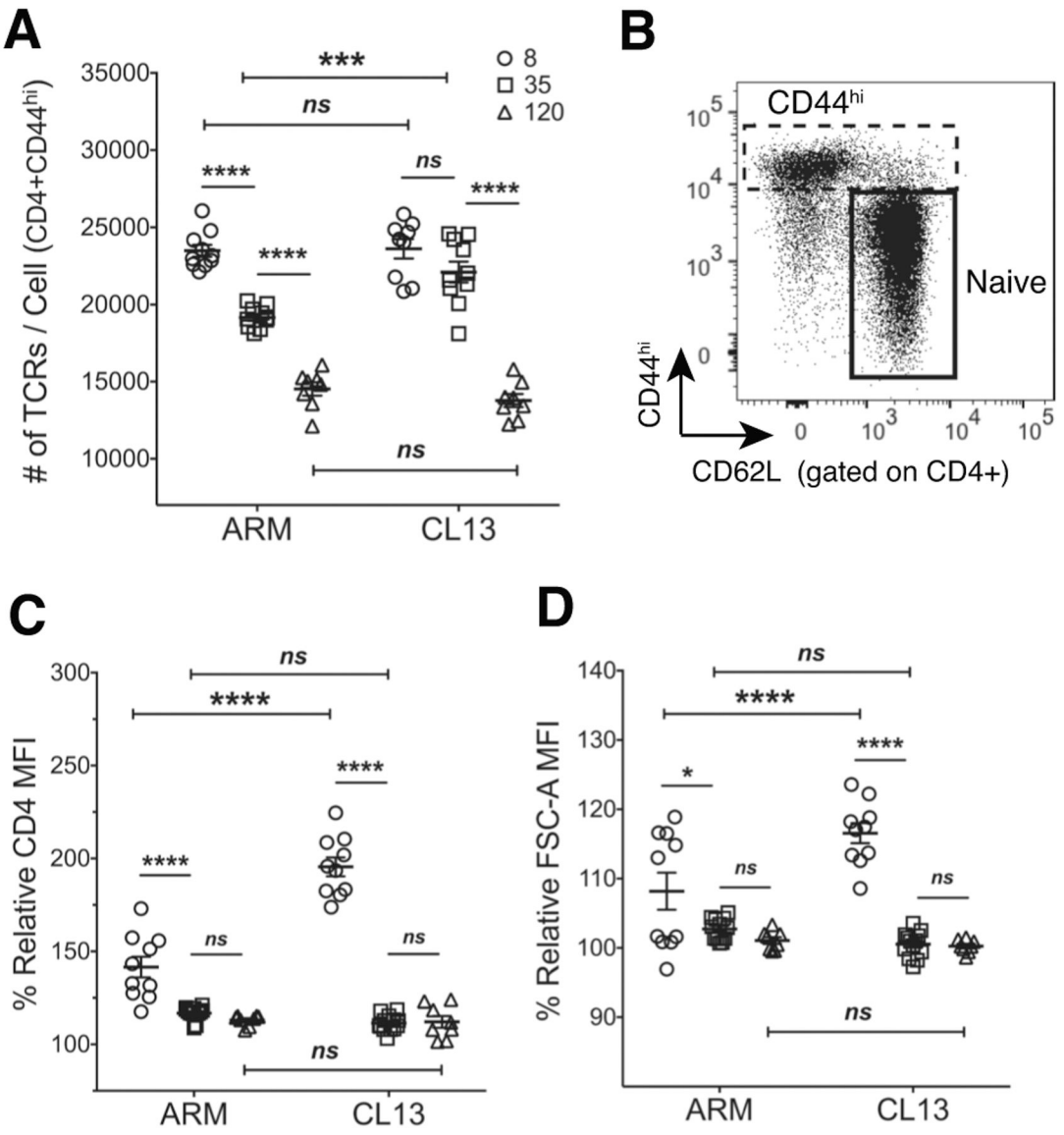

Figure 3. TCR expression higher in CL13 infection.

(A) TCRβ per cell numbers for CD44^{hi} CD4 T cells from ARM and CL13 infected splenocytes at the designated days using PE quantification beads. **(B)** A representative flow plot showing the gating strategy for naïve (CD44^{lo}CD62L+) and antigen experienced (CD44^{hi}) cells from total CD4 T cells. **(C)** % CD4 MFI and **(D)** % FSC-A MFI of CD44^{hi} cells normalized to naïve MFIs. (A,C,D) Points representing individual mice (n=7–10 mice with n=2–5 mice/experiment/group). MFI of CD44^{hi} cells divided by MFI of naïve cells and multiplied by hundred to get % relative MFI. Mean ± SEM. Statistical significance, ns = no significance, ** P > 0.01, *** P > 0.001, **** P > 0.0001, Ordinary one-way ANOVA Tukey's multiple comparison test (between dpi - individual infections), Sidak's multiple comparison test (ARM vs CL13).

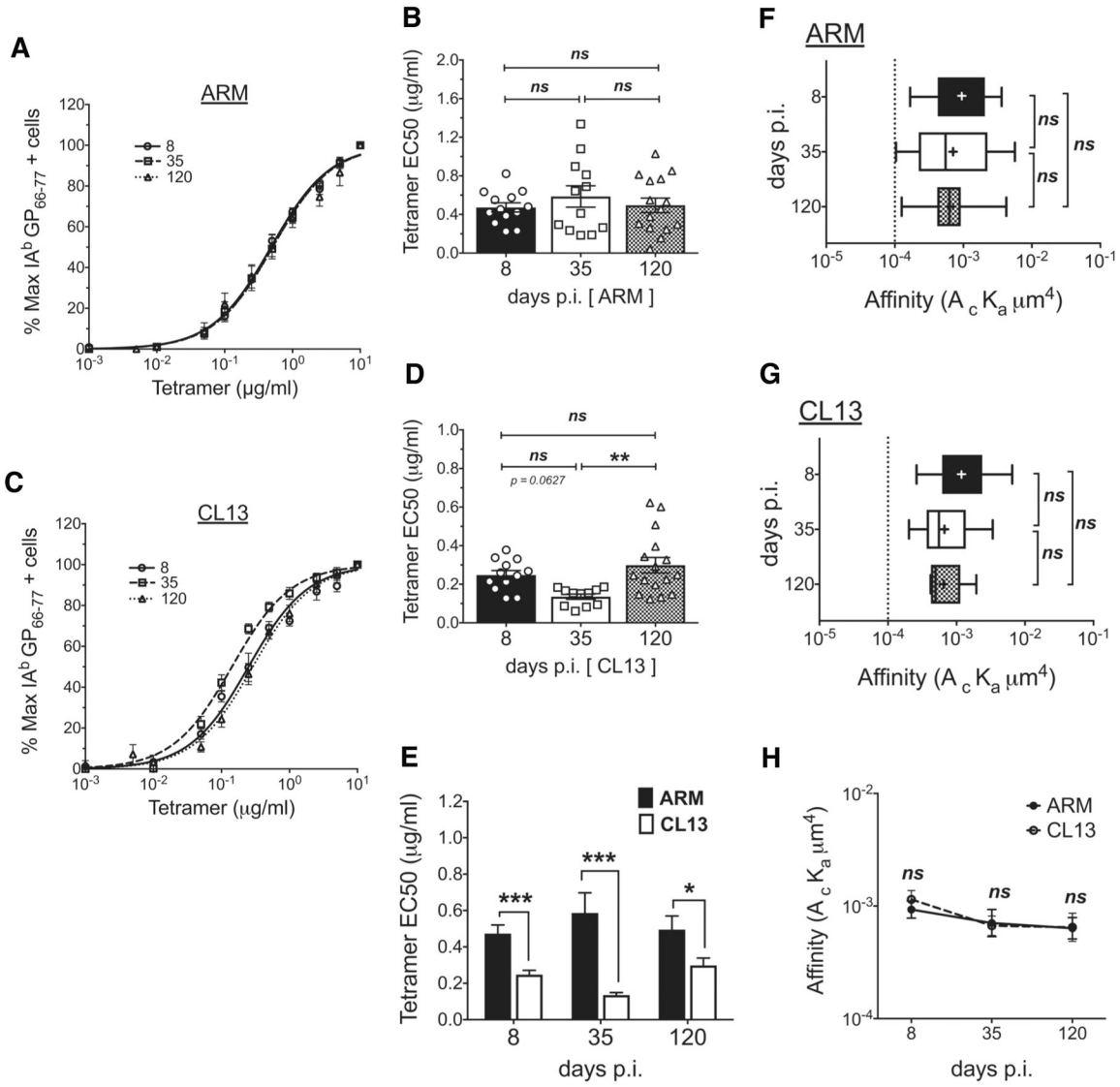

Figure 4. Tetramer avidity changes in chronic infection in the absence of TCR affinity differences.

Tetramer avidity curves showing % maximum tetramer+ cells at the different tetramer concentrations used to stain splenocytes from **(A)** ARM and **(C)** CL13 infected mice at the different dpi. The frequency of tetramer+ cells at the different doses was divided by the frequency at the highest concentration (10ug/ml) to calculate % maximum tetramer binders. Curves fitted to a non-linear regression (normalized frequency x log concentration - dose response curve with a variable slope). EC_{50} tetramer concentrations obtained from the dose response curves for individual mice from **(B)** ARM and **(D)** CL13 infections. **(E)** Comparison of EC_{50} values between ARM and CL13 at the different dpi. 2D affinity of antigen specific cells that fall above the tetramer staining affinity cutoff **(F)** ARM and **(G)** CL13 infection and **(H)** a comparison of the two responses. (A,C) Curves represent the Mean ± SEM of n = 12–16 mice. (B,D,E) Mean ± SEM in bar graphs with n=8–12 mice with each symbol representing individual mice. (F,G,H) pooled sample from 2–3 mice, affinity data log transformed with (+) sign depicting mean affinity in box and whisker graphs

with min to max range of measured single cell affinities. Tetramer + high affinity cell cutoff as a dotted line at 1×10^{-4}. All data representative of 3–5 independent experiments at n=2–5 mice/experiment/group. Statistical significance, ns = no significance, * P > 0.05, ** P > 0.01, *** P > 0.001, **** P > 0.0001, (B, D, F, G) Ordinary one-way ANOVA Tukey's multiple comparison test (between dpi - individual infections), (E) Student t-test, (H) Sidak's multiple comparison test (ARM vs CL13).

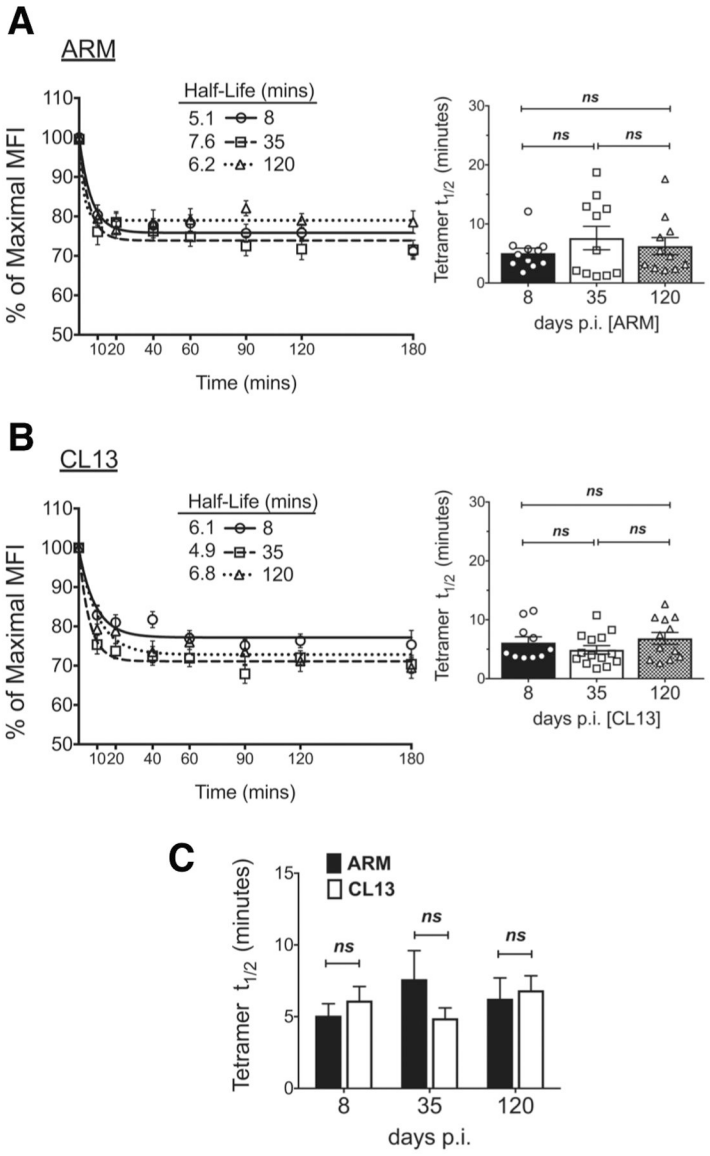

Figure 5. Tetramer half-life similar between memory and exhausted CD4 T cells.

Tetramer decay curves (left) and bar graphs of half-lives (right) for CD4 T cells from **(A)** ARM and **(B)** CL13 infected splenocytes and **(C**) a comparison of the two shown for the different dpi. (A, B left) Tetramer MFI at decay time points was normalized to time 0 MFI and the % MFI fitted to a one-phase exponential decay curve. (A,B right) Half-lives derived from curves for individual mice in bar graphs with symbols representing each mouse. Mean ± SEM representative of n = 13–14 mice, 3–5 independent experiments at n=3–5 mice/ experiment/group. Statistical significance, ns = no significance. (A,B) Ordinary one-way ANOVA Tukey's multiple comparison test (between dpi - individual infections), (C) Student t-test (ARM vs CL13).

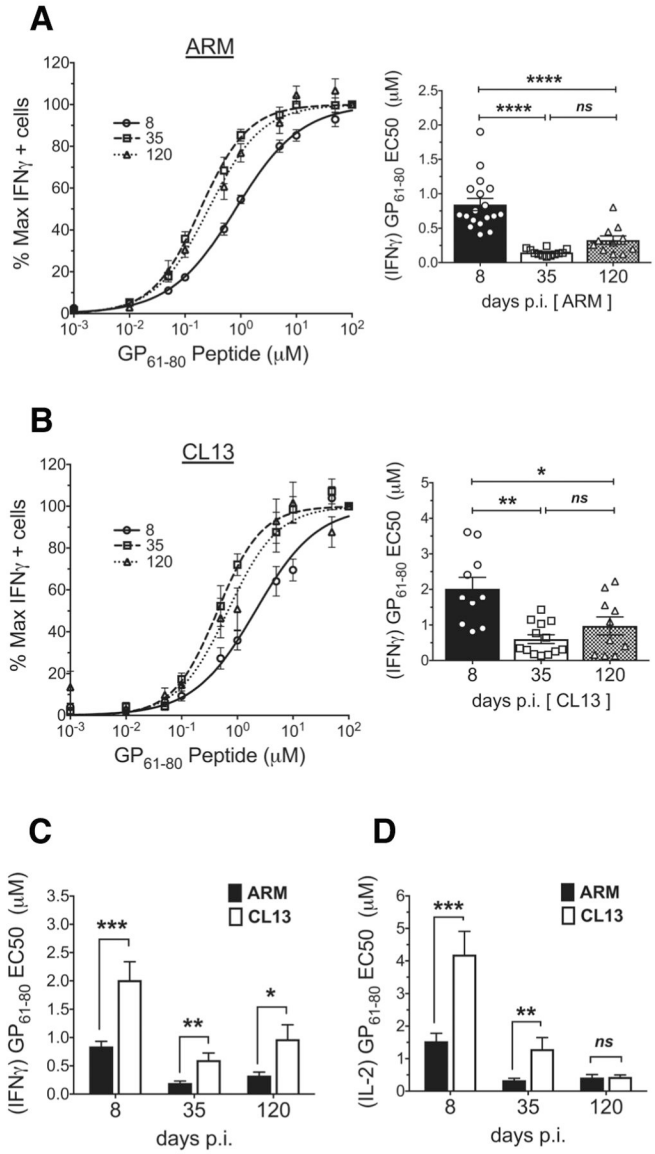

Figure 6. Exhausted CD4 T cells have a lower functional avidity compared to memory cells.

Functional avidity dose response curves showing % of maximal IFN**γ** producers at the different doses of $GP_{61–80}$ peptide used for ex-vivo stimulation of splenocytes from **(A,** left**)** ARM and **(B,** left**)** CL13 infected mice at the different dpi. The frequency of IFN**γ** producers at the different doses was divided by the frequency of producers at the highest peptide dose (100uM) to calculate % maximal producers. Curves fitted to a non-linear regression (normalized frequency x log concentration - dose response curve with a variable slope). EC_{50} peptide concentrations derived from the dose response curves for individual mice represented in bar graphs with each symbol representing a mouse for **(A,** right**)** ARM and **(B,** right**)** CL13. **(C)** Comparison of IFN**γ** and **(D)** IL-2 EC_{50} values between ARM and CL13 at the different dpi. Mean ± SEM (A,B,C) representative of n = 9–18 mice and (D) n=7–10 mice. 3–5 independent experiments at n=2–5 mice/experiment/group. Statistical significance, ns = no significance, * P > 0.05, ** P > 0.01, *** P > 0.001, **** P > 0.0001,

(A,B right) Ordinary one-way ANOVA Tukey's multiple comparison test (between dpi - individual infections), (C, D) Student t-test (ARM vs CL13).